NEOPLASIA
www.neoplasia.com

Volume 23 Number 3 March 2021 pp. 294–303

Original Research

Optical scattering as an early marker of apoptosis during chemotherapy and antiangiogenic therapy in murine models of prostate and breast cancer ☆

Syeda Tabassum [a]; Anup Tank [b]; Fay Wang [b]; Kavon Karrobi [b]; Cameron Vergato [c]; Irving J. Bigio [a,b]; David J. Waxman [c]; Darren Roblyer [a,b,*]

[a] Electrical & Computer Engineering, Boston University, Boston, MA, USA
[b] Biomedical Engineering, Boston University, Boston, MA, USA
[c] Division of Cell and Molecular Biology, Department of Biology and Bioinformatics Program, Boston University, Boston, MA, USA

Abstract

Monitoring of the in vivo tumor state to track therapeutic response in real time may help to evaluate new drug candidates, maximize treatment efficacy, and reduce the burden of overtreatment. Current preclinical tumor imaging methods have largely focused on anatomic imaging (e.g., MRI, ultrasound), functional imaging (e.g., FDG-PET), and molecular imaging with exogenous contrast agents (e.g., fluorescence optical tomography). Here we utalize spatial frequency domain imaging (SFDI), a noninvasive, label-free optical technique, for the wide-field quantification of changes in tissue optical scattering in preclinical tumor models during treatment with chemotherapy and antiangiogenic agents. Optical scattering is particularly sensitive to tissue micro-architectural changes, including those that occur during apoptosis, an early indicator of response to cytotoxicity induced by chemotherapy, thermotherapy, cryotherapy, or radiation therapy. We utilized SFDI to monitor responses of PC3/2G7 prostate tumors and E0771 mammary tumors to treatment with cyclophosphamide or the antiangiogenic agent DC101 for up to 49 days. The SFDI-derived scattering amplitude was highly correlated with cleaved caspase-3, a marker of apoptosis ($\rho_p = 0.75$), while the exponent of the scattering wavelength-dependence correlated with the cell proliferation marker PCNA ($\rho_p = 0.69$). These optical parameters outperformed tumor volume and several functional parameters (e.g., oxygen saturation and hemoglobin concentration) as an early predictive biomarker of treatment response. Quantitative diffuse optical scattering is thus a promising new early marker of treatment response, which does not require radiation or exogenous contrast agents.

Neoplasia (2021) 23, 294–303

Keywords: Imaging, Spectroscopy, Optical scattering, Treatment monitoring, Apoptosis, Cell proliferation

Introduction

Surveillance of the in vivo tumor state during the course of drug treatment is essential for understanding the efficacy of anticancer agents in the preclinical setting [1]. Preclinical imaging methods can help to identify and validate promising new treatments, test multi-agent regimens, and optimize the scheduling and dosing of emerging therapies [2]. Available preclinical imaging techniques focus on anatomic imaging, function or metabolic imaging, or molecular imaging with exogenous agents [1,3]. Here we focus on optical scattering as a novel marker of anticancer therapy response.

Optical scattering occurs as a consequence of the specific tissue microarchitecture within cells, subcellular structures, and the tumor microenvironment [4,5]. Importantly, optical scattering is sensitive to tissue micro-architectural changes that occur during apoptosis and proliferation

* Corresponding author.
E-mail address: roblyer@bu.edu (D. Roblyer).

☆ *Abbreviations:* AUC, area under the curve, CPA, cyclophosphamide, DOI, diffuse optical imaging, IHC, Immunohistochemistry, NIRS, Near-Infrared Spectroscopy, SFDI, spatial frequency domain imaging, TV, tumor volume.

Received 19 October 2020; received in revised form 12 January 2021; accepted 26 January 2021

https://doi.org/10.1016/j.neo.2021.01.005

[6–8], given that most therapeutically effective cytotoxic anticancer agents induce apoptosis [9–11]. In fact, the successful elimination of cancer cells by any nonsurgical means (chemotherapy, thermotherapy, cryotherapy, or radiation therapy) inevitably invokes large-scale apoptosis [12]. In contrast to other forms of cell death, apoptosis exhibits unique micromorphology changes, especially in early stages, wherein apoptotic changes in the cell nucleus are well established. In apoptotic cells, nuclear material (chromatin) condenses into coarsely granular aggregates, either distributed over the entire nucleus or localized to crescent-shaped arcs at the interior surface of the nuclear membrane [13]. At later stages, in most, but not all cases, the nucleus then breaks up into discrete fragments that maintain the characteristic segmentation of chromatin [14]. Significant morphological changes also occur in mitochondria during the early stages of apoptotic cell death, including swelling [15] and shrinkage [16]. These micromorphological changes in turn lead to significant changes in the optical scattering properties of apoptotic cells [4,17].

While optical scattering is potentially promising as a label-free contrast mechanism for monitoring apoptosis and therapy response, until recently there has not been a method to quantify optical scattering over a wide-field, such as over the tumor surface in preclinical tumor models. Here, we exploit spatial frequency-domain imaging (SFDI), a new wide-field and label-free imaging modality that utilizes spatially-modulated optical illumination, to quantify optical scattering and absorption in the red-to-near-infrared wavelength band (600−1000 nm) [18]. We use SFDI to longitudinally track prostate and breast tumors in mouse models during treatment with cytotoxic and antiangiogenic agents. SFDI quantifies optical scattering, and absorption due to tissue chromophores, including oxyhemoglobin and deoxyhemoglobin. These features differentiate SFDI from other wide-field modalities, including molecular imaging strategies that require exogenous contrast agents, optical coherence tomography, which images a small area, and photoacoustics, which provides no scattering contrast. SFDI belongs to a larger class of diffuse optical imaging (DOI) techniques, many of which have been translated to the clinic for diagnostic and prognostic applications in breast, prostate, and other solid tumors [19–23].

We set 2 goals for the present work: (1) to determine the ability of optical scattering to predict early treatment response in clinically-relevant tumor models; and (2) to investigate the biological correlates of optical scattering and other SFDI metrics in drug-treated versus control tumors. To accomplish these goals, we first tracked scattering-based parameters in prostate and breast xenograft models following cytotoxic drug and antiangiogenic agent treatment. We then correlated SFDI metrics with tumor physiological markers in a cross-sectional animal study conducted over multiple weeks. Finally, we compared the utility of optical scattering as an early marker of treatment response against other commonly utilized parameters, including anatomic tumor volume (TV) and functional measurements (e.g., tumor oxygen saturation).

Materials and methods

Spatial frequency domain imaging

Detailed descriptions of SFDI instrumentation and data analysis are provided elsewhere [1,2,24,41], and additional details are provided in Supplementary Methods. Briefly, SFDI utilizes projections of spatially modulated visible and/or NIR light to extract intrinsic tissue optical properties (absorption and reduced scattering coefficients, μ_a and μ'_s) over a wide field of view. Fig. 1 shows a simplified schematic of the SFDI system (left panel), as well as SFDI processing steps (right panel). The λ- and spatial frequency (f_x)-dependent instrument response function is determined using a calibration procedure, which involves the measurement of a tissue-simulating phantom with known μ_a and μ'_s values over the range of wavelengths of the system. This calibration was repeated on each measurement day to account for any day-to-day variation in the instrumentation. The demodulated images were then calibrated to obtain tissue diffuse reflectance (R_d) maps.

A power law was fit to the μ'_s values at each of the 4 instrument wavelengths using a least-squares fitting approach to derive the scattering amplitude (a) and scattering power (b) as denoted in Eq. 1, for each spatial location within the field of view.

$$\mu'_s(\lambda) = a\left(\lambda/\lambda_o\right)^{-b} \quad (1)$$

A reference wavelength (λ_o) of 800 nm was used in the power-law fitting, where a is the value of μ'_s at $\lambda = \lambda_0$. The extracted values of μ_a, were used to derive tissue chromophore concentrations using Beer's Law (Eq. 2).

$$\mu_a(\lambda) = \varepsilon_{HbO_2}(\lambda) * ctHbO_2 + \varepsilon_{Hb}(\lambda) * ctHb \quad (2)$$

This equation utilizes the measured μ_a values and the known chromophore extinction coefficients for oxyhemoglobin ($\varepsilon_{HbO_2}(\lambda)$) and deoxyhemoglobin ($\varepsilon_{Hb}(\lambda)$), and is solved as a linear system of equations to yield tissue-level concentrations of oxyhemoglobin ($ctHbO_2$) and deoxyhemoglobin (ctHb). From these, additional hemodynamic parameters are indirectly derived, including total hemoglobin content ($ctTHb = ctHbO_2 + ctHb$) and oxygen saturation ($StO_2 = (ctHbO_2/ctTHb) \times 100$).

Cell lines, animals, and treatment details

Five- to 6-week-old male (21−23 g) severe combined immunodeficient (SCID) hairless outbred mice (SHO-*Prkdc*^{scid}*Hr*^{hr}; Charles River Laboratories) bearing PC3/2G7 tumors [25] were randomly assigned to treatment groups when the average group TV reached ∼500 mm^3: control (drug-free) group, N=33 mice; cyclophosphamide (CPA) treatment, $N = 25$ mice; DC101 treatment, $N = 29$ mice. Mice were treated with CPA or with DC101 by intraperitoneal injections or were left untreated in the case of the control group. CPA monohydrate was administered on a metronomic schedule at 150 mg/kg every 6 days for 3 cycles. DC101 was given at 28.6 mg/kg every 3 days for 6 cycles. In a separate study, mouse E0771 mammary tumors were implanted orthotopically in 6-week-old (15−18 g) female C57BL/6 mice (#B6-F, Taconic Biosciences, Rensselaer, New York) ($N = 13$ mice). The E0771 model was included to contrast observed trends in optical changes seen in PC3/2G7 tumors against a second tumor type. Mice were randomized to control ($N = 4$), CPA ($N = 4$) and DC101 ($N = 5$) treatment groups when the average TV reached ≥250 mm^3. CPA monohydrate was administered on a metronomic schedule at 139 mg/kg every 6 days for 2 cycles. DC101 was administered at 40 mg/kg every 3 days for 3 cycles. The control group received nonspecific mouse IgG (Jackson Immuno Research Laboratories) at 40 mg/kg every 3 days for 3 cycles. All treatments were given by intraperitoneal injection. During SFDI measurements, mice were anesthetized by isoflurane inhalation (5% induction). Immunohistochemistry (IHC) and tissue image analyses are described in Supplementary Methods.

Longitudinal monitoring with SFDI

SCID mice bearing PC3/2G7 tumors were monitored longitudinally with SFDI over a 22-day period of tumor growth prior to drug treatment, and then for 27 days after the start of treatment. Mice were imaged every 3 days prior to drug treatment, at least twice every 3 days during the 18 days of treatment, and every 3 days during the post-treatment tumor rebound period. Mice were assigned to 3 groups at the start of treatment: control, CPA and DC101. Several SCID mice from each group were euthanized for tissue analysis on days 0, 1, 9, 18, and 26 (at least $N = 4$ per group on each day; Supplementary Fig. S2B). Day 0 (baseline) was the first treatment day. Tumors were frozen or fixed for cross-sectional analysis by IHC. Some SCID mice ($N = 12$) were monitored up to 69 days after initiating treatment for movie visualizations to illustrate finer temporal resolution and longer-term trends. C57BL/6 mice bearing E0771 tumors were imaged with SFDI on days 0, 3, 6, and 9.

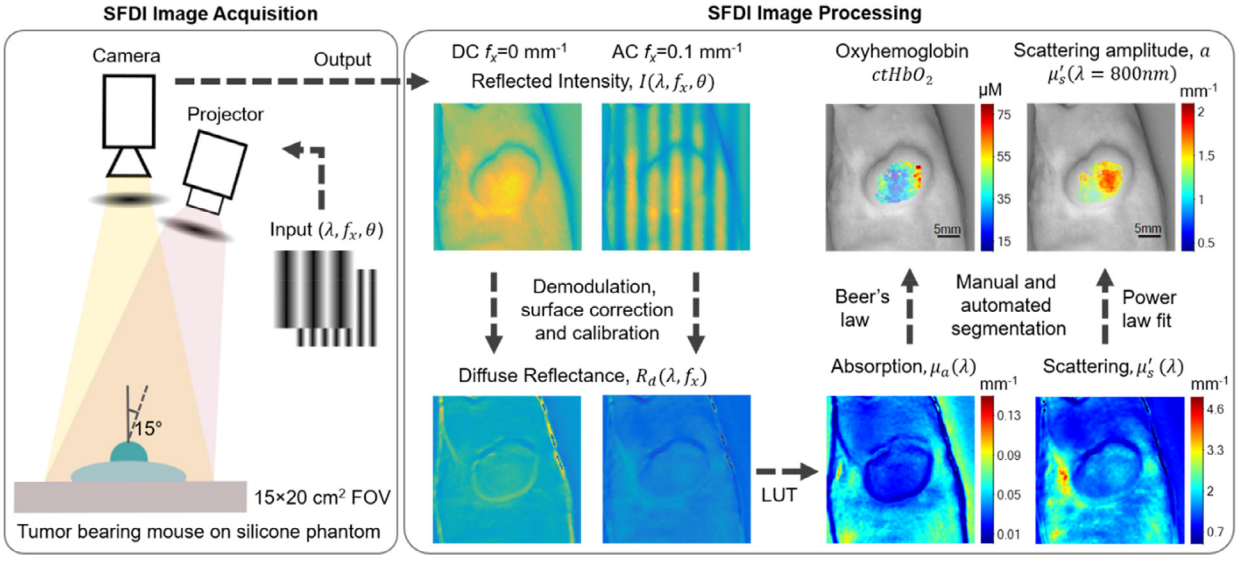

Fig. 1. The left panel shows a simplified schematic of the SFDI system. Sinusoidal 1-D patterns of light at multiple wavelengths (λ), spatial frequencies (f_x), and phases (θ) are projected onto a sample of interest, and the reflected intensity is collected with a CCD camera. The right panel shows the SFDI processing pipeline for representative PC3/2G7 tumor measurements. The intensity images (I) at λ = 731 nm are shown for 2 spatial frequencies (f_x: 0 mm^{-1} (DC) and 0.1 mm^{-1} (AC)). Diffuse Reflectance (R_d) maps are computed after demodulation, height and angle correction, and calibration steps. The absorption ($\mu_a(\lambda)$) and reduced scattering ($\mu'_s(\lambda)$) maps are then determined using a precomputed Look-up-table (LUT) that maps multi-frequency R_d to optical properties at each pixel in the image. Edge artifacts are removed through automated and manual segmentation. Chromophore values are then determined using Beer's Law, and the wavelength dependence of optical scattering is fit to a power law. Oxyhemoglobin ($ctHbO_2$) and scattering amplitude (a) are shown for the tumor area superimposed on a grayscale image. SFDI, spatial frequency domain imaging.

Results

Optical scattering reveals dynamic changes in control and treated tumors

Tumor growth stasis was induced by treatment of PC3/2G7 tumors with either CPA or DC101 (Supplementary Fig. S2A). Longitudinal visualizations of SFDI parameters revealed substantial changes in optical parameters during drug treatment, especially changes in optical scattering. Fig. 2 shows scattering amplitude (a) maps (μ'_s at λ = 800 nm) for representative tumors in each group over a 27-day observation period. The day-0 values were set to the middle of the color-bar range to highlight both increases (*red*) and decreases (*blue*) from baseline. For control tumors, a decreased with increasing TV throughout the 27-day period. For CPA-treated tumors, where volume increases were substantially inhibited, a increased, in stark contrast to the control group. Similarly, for the DC101-treated tumors, volume increases were largely suppressed while a increased significantly through day 27. Time-course videos highlight similar changes with finer temporal resolution (Supplementary Fig. S3). Less prominent contrast was observed in absorption-based hemodynamic parameters, such as $ctHbO_2$, ctHb, ctTHb, and StO_2.

Optical scattering parameters correlate with apoptosis and proliferation

Optical scattering is sensitive to microarchitectural changes at the cellular and sub-cellular levels, and is likely to be correlated with treatment-induced biological changes [26,27]. Prior work from our labs reported detailed changes in the Mie-theory parameters for scattering from cancer-cell cultures due to chemotherapy-induced apoptosis [4,17]. Here, for our in vivo studies, we explored how reduced scattering coefficient and other SFDI-derived parameters relate to the underlying tumor biology in macroscopic tissue. To this end, our in vivo SFDI imaging data of PC3/2G7 xenografts was interpreted in the context of changes in IHC markers for apoptosis (cleaved caspase-3), cell proliferation (PCNA), blood vessel density (CD31), glucose uptake (Glut-1), macrophage infiltration (Mac-1), and vessel patency (leakiness: Hoechst assay). Table 1 summarizes the SFDI optical parameters and IHC biomarkers, along with our hypotheses for potential correlations and references to previous literature supporting the proposed correlations. For example, prior work in scattering spectroscopy and optical coherence tomography (integrated backscatter) demonstrated a positive correlation between scattering amplitude and apoptosis [6,7,26,27]. Additionally, clinical DOI and preclinical optical coherence tomography studies have shown a reduction in the wavelength dependence of scattering (i.e., the scattering exponent (b)) as a marker of treatment response [728,29].

Fig. 3 shows longitudinal changes in the SFDI parameters paired with changes in TV and IHC results. Treatment continued from day 0 (baseline measurements) to day 18, while days 24, 26, and 27 represent the post-treatment rebound period (Fig. 3B). Correlations between key imaging and IHC metrics are also shown.

The scattering amplitude parameter, a, decreased in the control group but increased significantly in the treated groups, with both CPA and DC101, during treatment and rebound (Fig. 3C). The scattering power exponent, b, also displayed longitudinal trends in the treatment groups, with significant decreases observed during treatment and rebound (Fig. 3F). The longitudinal patterns observed in the a parameter were broadly correlated with changes in cleaved caspase-3, as indicated by the large increases in a in both the CPA and DC101 groups (Fig. 3D). The changes in the b parameter were likewise correlated with the PCNA trends, with significant decreases in b observed in both treatment groups (Fig. 3G). The correlations of the daily group mean of these scattering and IHC parameters were also strong for a versus cleaved caspase-3 (Fig. 3E, Pearson correlation coefficient (ρ_p) = 0.75 [unadjusted $P < 0.01$, TCH adjusted $P < 0.0085$]) and b versus PCNA (Fig. 3H, $\rho_p = 0.69$ [unadjusted $P < 0.01$, TCH adjusted $P < 0.0085$]). Cleaved caspase-3 and

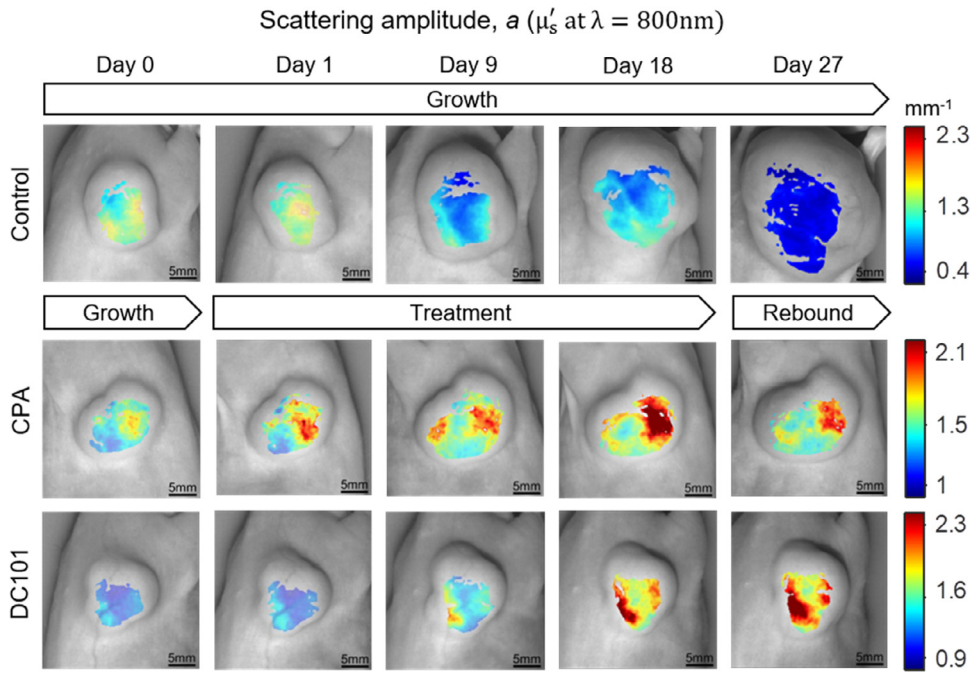

Fig. 2. Longitudinal changes in scattering amplitude (*a*) maps (μ'_s at $\lambda = 800$ nm) for representative control, CPA-treated, and DC101-treated PC3/2G7 tumors on the days indicated. CPA, cyclophosphamide.

Table 1

Exploratory correlations between SFDI optical parameters and IHC biomarkers.

	IHC and SFDI Correlative Analysis in Tumor Models	
SFDI optical marker	**IHC marker**	**Physiological basis for SFDI vs. IHC correlation**
Scattering amplitude (*a*)	Apoptosis (cleaved caspase-3)	Cell break down, chromatin condensation, and mitochondrial changes during apoptosis increase the density of optical scattering centers, resulting in an increase in scattering amplitude [4,6,7,17].
Scattering exponent (*b*)	Cell proliferation (PCNA) and apoptosis (CC3)	The increase in cell density during proliferation alters the distribution of scattering particle sizes, causing *b* to increase; apoptotic volume decreases and chromatin and mitochondrial changes during apoptosis cause *b* to decrease [4,7,17,28,29].
Oxyhemoglobin ($ctHbO_2$) Total hemoglobin (ctTHb) Oxygen saturation (StO_2)	Blood vessel density (CD31), Blood vessel patency (Hoechst assay)	A higher number of functional vessels results in increased blood distribution in the tumor, which increases Oxyhemoglobin, Total Hemoglobin, and in some cases, Oxygen Saturation [8,28,29].
Deoxyhemoglobin (ctHb)	Cell proliferation (PCNA), glucose uptake (Glut1)	Increases in cell proliferation lead to increases in oxygen consumption due to higher metabolic activity, causing an increase in ctHb [28,29].

IHC = immunohistochemistry; SFDI = spatial frequency domain imaging.

PCNA values at day 26 were plotted against *a* and *b* at day 24, since no SFDI measurements were taken on day 26, and *a* and *b* at day 27 were excluded from the correlation analysis due to the small number of tumors in the CPA group at that time point ($n = 2$). Of note, the drop in *a* and the increase in *b* on day 27 in the CPA group coincides with the tumor rebound period and with an increase in the average TV (Fig. 3A, Supplementary Fig. S2A). This may be an indication of tumor regrowth after treatment, although the small number of tumors at that time point ($n = 2$) limits the significance.

Trends similar to those seen for the *a* parameter in the CPA-treated PC3/2G7 model were seen for CPA-treated E0771 tumors implanted in C57BL/6 mice (Supplementary Fig. S4A). Although the *b* parameter did not show a statistically significant decrease in the treated groups, the CPA group showed a decreasing trend compared to control (Supplementary Fig. S4C). The DC101 group did not show a therapeutic response to DC101 over the 9-day observation period, and correspondingly, we did not see a trend in the *b* parameter (Supplementary Fig. S4B, D).

Hemodynamic parameters correlate with vessel density and patency

Clinical studies have demonstrated that ctTHb and $ctHbO_2$ both decrease during successful treatment of breast cancer patients with neoadjuvant chemotherapy [28,29]. Further, there is a positive correlation between ctTHb and mean vessel area in breast cancer patients [30,31]. Here, we observed significant decreases in ctTHb and $ctHbO_2$ in both treated and control groups (Fig. 3I and Supplementary Fig. S5A), and significant decreases in ctHb were observed in the DC101 treatment group (Supplementary Fig. S5C). We hypothesized that the extent of functional vessels revealed by the Hoechst assay were likely to be correlated with blood volume and ctTHb. This relationship was most apparent in the DC101 group, where significant decreases in Hoechst staining were seen on days 9 and 18. The correlation between ctTHb and Hoechst staining is shown in Fig. 3K ($\rho_p = 0.54$, unadjusted $P < 0.05$, insignificant TCH adjusted *P* value).

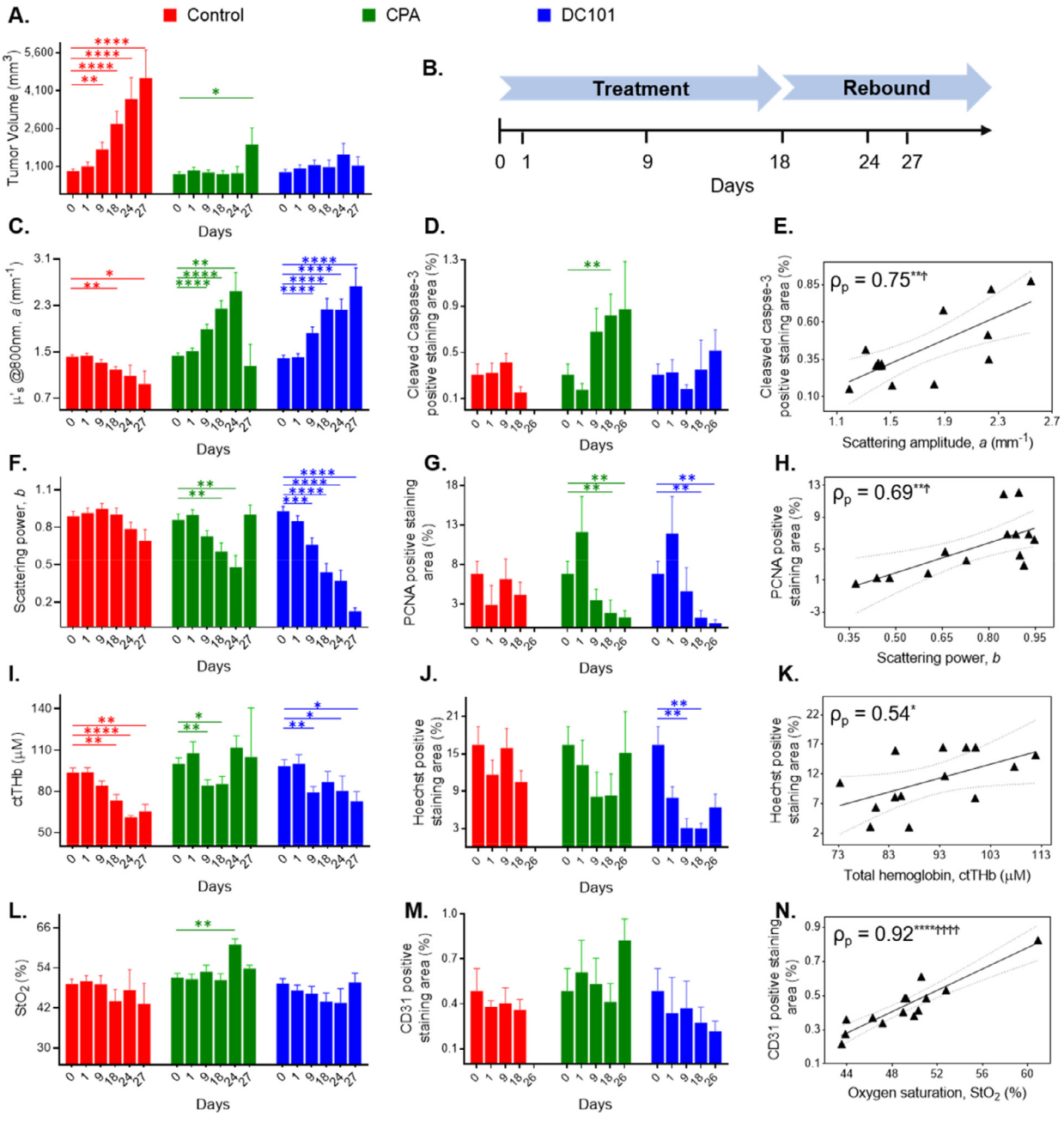

Fig. 3. (A) Longitudinal changes in PC3/2G7 tumor volume. (B) A simplified timeline of the study. Longitudinal changes in the SFDI parameters (C, F, I, L) paired with IHC results (D, G, J, M) in PC3/2G7 tumors on representative days. Data in the bar plots represent mean and standard error in each group. The number of tumors at each time point decreased over time as mice were euthanized for IHC analysis (Supplementary Fig. S2B). The Mann-Whitney Wilcoxon rank sum test was used to test if longitudinal SFDI and IHC metrics were statistically different from baseline (day 0) values. Relationships between SFDI and IHC metrics are shown in E, H, K, N using daily group means from the bar plots. The linear best fit and 95% confidence intervals are indicated. The Pearson's ρ (ρ_p) is reported for each plot, along with significance range using both unadjusted and Tukey-Ciminera-Heyse TCH-adjusted P-values. *, significance range with unadjusted P values; †, significance range with TCH adjusted P-values. Here, *, $P < 0.05$; **, $P < 0.01$; ***, $P < 0.001$; ****, $P < 0.0001$; †, $P < 0.0085$; ††††, $P < 0.0000166$. IHC, immunohistochemistry; SFDI, spatial frequency domain imaging.

None of the changes in StO_2 were statistically significant except for day 24 in the CPA group. There were no significant changes in CD31 staining. However, both parameters showed similar trends, with decreases in the DC101 groups and spikes seen in the rebound period in the CPA group, resulting in a strong overall linear correlation between StO_2 and CD31 (Fig. 3N, $\rho_p = 0.92$ [unadjusted $P < 0.0001$, TCH adjusted $P < 0.0000166$]).

The remaining longitudinal trends and correlations are shown in Supplementary Fig. S5. The trends in both $ctHbO_2$ and ctHb were similar to the trends in ctTHb, with decreases observed in control and DC101 treatment groups, as well as a spike during rebound in the CPA group. Decreases in the glucose transporter Glut-1 were observed in the CPA group, while increases were observed in the DC101 group. Large increases in macrophage infiltration were observed with DC101 treatment. We also

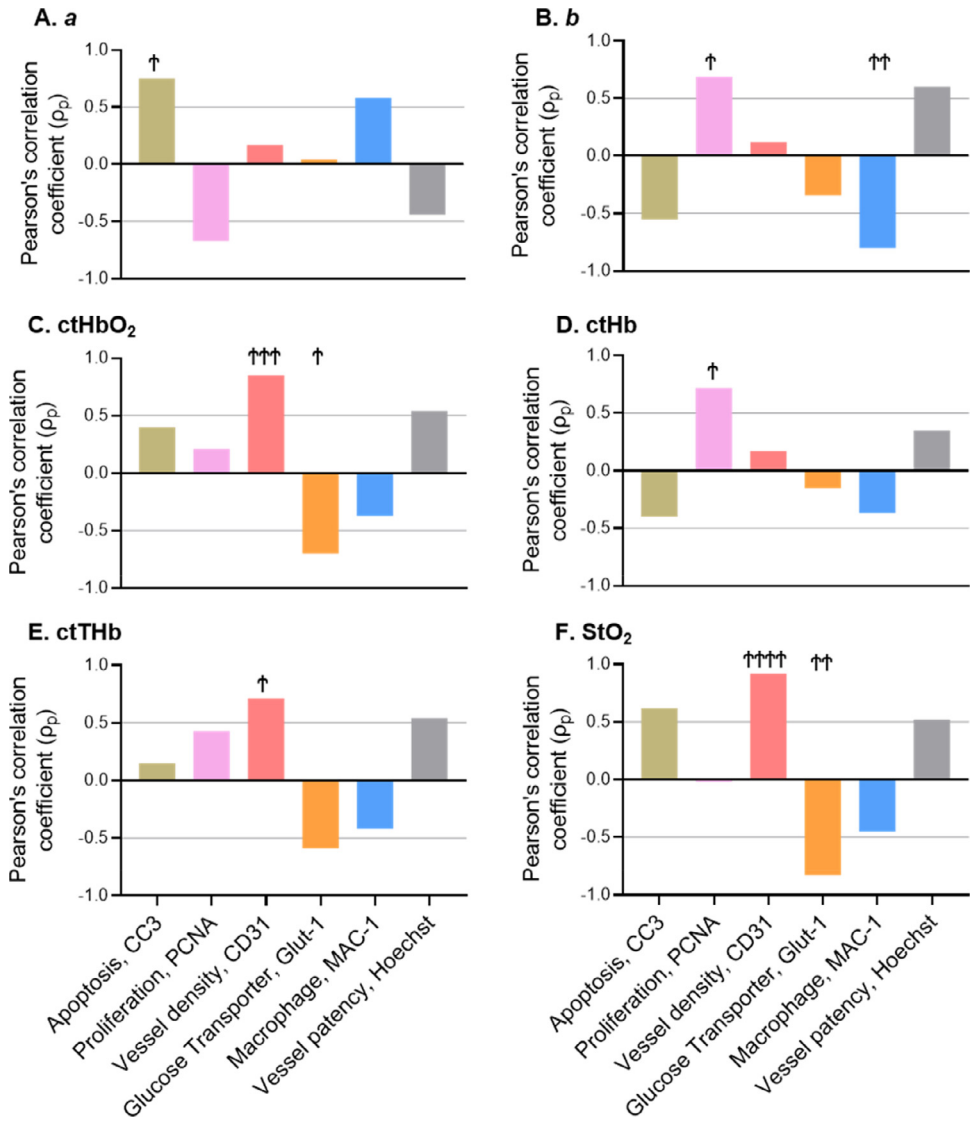

Fig. 4. Pearson's ρ (ρ_p) values for each SFDI and IHC marker. † Denotes significance using TCH adjusted P values: $P < 0.0085$; ††, $P < 0.0017$; †††, $P < 0.000167$; ††††, $P < 0.0000166$. IHC, immunohistochemistry; SFDI, spatial frequency domain imaging.

note that StO_2 and Glut-1 were strongly correlated, $\rho_p = -0.83$ (unadjusted $P < 0.001$, TCH adjusted $P < 0.0017$); the b parameter and Mac-1 were strongly correlated, $\rho_p = -0.8$ (unadjusted $P < 0.001$, TCH adjusted $P < 0.0017$); and the ctHb parameter was strongly correlated with PCNA, $\rho_p = 0.72$ (unadjusted $P < 0.01$, TCH adjusted $P < 0.0017$). The drop in StO_2 with higher Glut-1 and the increase in ctHb with higher PCNA may both reflect the fact that increased proliferation leads to increased oxygen consumption and a buildup of ctHb [29]. A summary of the Pearson's ρ (ρ_p) values for each SFDI and IHC marker is presented in Fig. 4. Based on our mechanistic hypotheses, and considering prior literature supporting these correlations (Table 1), we propose that these correlations represent, at least in part, causative links rather than merely associations.

Optical scattering provides high contrast between treated and control tumors

Imaging parameters that provide high contrast between responding and nonresponding patients at early time points during cancer therapy have the potential for high utility for monitoring of response to treatment [32]. Here we explored optical biomarkers for contrast between treated tumors, compared to untreated tumors as a surrogate for lack of clinical response. Tumor values were first normalized to day-0 (baseline) values. The $\log_2$ ratio of tumor to control optical properties and TV are plotted over the duration of the study (Supplementary Fig. S6). For CPA, TV gave the largest average contrast between treated and control tumors over the study, but the a and b scattering parameters also provided high contrast (Supplementary Fig. S6A). The contrast in these parameters continued to increase throughout the study. These trends were similar for DC101, where the parameter b performed almost as well as TV (Supplementary Fig. S6B). In contrast, the hemodynamic parameters ($ctHbO_2$, ctHb, ctTHb, StO_2) were not statistically significant on most days examined (Supplementary Fig. S6C, D). Based on these findings, we explored how SFDI parameters could be used either as a stand-alone marker, or as a companion marker to anatomic tumor size to predict treatment response at early time points.

Scattering parameters provide a superior and biologically-specific early response prediction compared to tumor volume and hemodynamic parameters

Discriminant analysis was conducted to determine the accuracy of classifying treated versus control tumors using SFDI parameters as either stand-alone imaging markers, or as companion markers to anatomic tumor size. The control tumors here serve as a preclinical stand-in for treated but nonresponding tumors, which are common in the clinical setting. While imperfect, this surrogate allows for the identification of SFDI markers that may provide early predictive accuracy if clinically validated. TV is used here to contextualize the predictive value of SFDI parameters, as it is widely used to track treatment response in the preclinical setting. In this analysis, tumor values were normalized to day 0 (baseline) and only time points within the treatment period (through day 18) were considered. Classification was conducted using single features and sets of 2 features. Classification for each individual feature and set of features was repeated 101 times and the median performing classifier (determined by the area under the curve (AUC) of a receiver operating characteristic (ROC) curve) was used for comparisons on individual days. The single feature and the feature combination that gave the highest average AUC over all measurement days were defined as the best feature sets.

A summary of classifier performance for several well performing single SFDI features and TV on different study days is shown in Fig. 5. For CPA, the scattering parameter *a* yielded better performance than TV on days 1 and 4. When *a* was combined with TV, superior performance was found on days 3 and 4 as compared to either parameter alone (shown in Supplementary Fig. S7A). For DC101, the exponent *b* provided the best performance on days 1 and 3, and *a* provided the best performance on days 4, 6, 7, and 9. The combination of *a* and TV had superior performance over either single feature on days 3, 4, 6, 7, and 9 (shown in Supplementary Fig. S7A).

At very early time points (i.e., days 1 and 4 for CPA; days 1, 3, and 4 for DC101) the stand-alone SFDI features *a* or *b* outperformed TV. This is also apparent in the ROC curves shown in Supplementary Fig. S7B-G. Fig. 5C, D shows AUC values up to day 9 along with linear regression fits. The prediction advantage, defined as the number of days it takes for TV to reach the same AUC value obtained with the *a* or *b* parameter, was computed for each day using the regression fits. The SFDI prediction advantage (in days) is plotted in Fig. 5E, F. Here, a positive predictive advantage indicates that the SFDI feature precedes TV by the indicated number of days, and a negative predictive value indicates the opposite. For CPA on day 1, the *a* parameter exhibited a positive predictive advantage of 1.4 days, meaning that within just 1 day of treatment, the *a* parameter provides a predictive power than is not matched by TV until after day 2 (Fig. 5E). This may be because the *a* parameter reflects early apoptotic events, which do not lead to decreased TV until tumor cell debris has been cleared. The *b* parameter yielded negative values for CPA, meaning this parameter does not provide a predictive advantage over TV on any day. For DC101, the *b* parameter yielded positive values as large as 2 days until day 4 (Fig. 5F). The *a* parameter for DC101 preceded TV starting at day 4. The fact that, at early time points, the *a* parameter is more effective for the CPA-treated tumors, while the *b* parameter is more effective for DC101-treated tumors may reflect the specific mechanism of each of these drugs (see Discussion).

Discussion

This work reports the utility of utilizing optical scattering for tracking tumor responses early during treatment of prostate and breast cancer xenografts, while simultaneously identifying histological and IHC correlates of SFDI-derived parameters. Two optical scattering parameters, the scattering amplitude (*a* parameter) and scattering power (*b* parameter), were identified as strong early predictors of treatment response. These parameters correlated strongly with markers for apoptosis and cell proliferation, respectively. Optical scattering thus has strong potential to meet the need for early, noninvasive oncologic imaging of markers of treatment response in preclinical tumor models. We now discuss the major results in the context of prior work, and address the limitations and potential of these findings to impact research and clinical care.

Trends in the *a* and *b* parameters for optical scattering were dramatically different between CPA-treated and DC101-treated tumors compared to controls. The scattering parameter *a* decreased in the control group but increased with both CPA and DC101 treatment. Concurrently, the *b* parameter decreased significantly during treatment. The scattering parameter *a* correlated strongly with IHC assays of cell apoptosis (cleaved caspase-3: $\rho_p = 0.75$) and the scattering *b* parameter correlated strongly with cell proliferation (PCNA: $\rho_p = 0.69$). Prior work utilizing modelling and cell culture experiments with optical scattering methods found distinct relationships between scattering amplitude (*a*) and the density of scattering centers, as well as scattering power (*b*), and the distribution of scattering particles sizes [26]. We hypothesize that as cells break down during apoptosis, the density of optical scattering centers increases due to morphological changes including chromatin condensation and mitochondrial changes, thereby increasing the *a* parameter. Consistent with this idea, the macrophage marker Mac-1 was positively correlated with the *a* parameter ($\rho_p = 0.58$), perhaps due to macrophage recruitment induced by clearance of dead cells after substantial apoptosis [33]. Additionally, apoptotic volume decreases caused by loss of cellular water during early apoptosis have been suggested to increase the optical index of refraction of the cytoplasm, resulting in an increase in scattering cross-section and a decrease in wavelength-dependent scattering parameter, *b*, as documented in our earlier in vitro work with the same cancer cell lines and cytotoxic agents reported here [4,17]. This is consistent with the increase in *a* and decrease in *b* parameters in treated tumors observed here. Conversely, during proliferation, an increase in cell density may alter the distribution of scattering particle sizes, leading to a higher proportion of smaller scattering centers, which causes *b* to increase [26]. Consistent with this work, studies using optical coherence tomography have shown an increase in integrated backscatter and a decrease in the scattering exponent in response to treatment in preclinical tumors [6,7], and clinical DOI tools revealed a decrease in the *b* parameter in breast cancer patients responding to treatment [28,29].

Both *a* and *b* scattering parameters provided high imaging contrast between treated and control tumors, starting at early time points. The classification analysis revealed the scattering *a* parameter as the best performing single SFDI feature for CPA, and $a + TV$ as the best performing dual feature during either treatment. Regression analysis demonstrated that the *a* parameter has a 1.4 day predictive advantage over TV in the first day after the start of treatment. These trends were different for DC101, where the *b* parameter exhibited a better prediction advantage than TV at the beginning of treatment, and the *a* parameter exhibited a better prediction advantage starting at day 4. We speculate that these differences reflect the different biological mechanisms of these drugs. CPA is an alkylating agent that can induce tumor apoptosis within hours of treatment [34], which plausibly leads to the predictive advantage of the *a* scattering parameter early during treatment. Conversely, DC101 targets vascular endothelial growth factor receptor 2, causing vessel regression, which conceivably inhibits proliferation before inducing apoptosis at later time points caused by oxygen and/or nutrient starvation. This may explain the early predictive power of the *b* parameter, followed later by the predictive power of the *a* parameter [25]. We also note that both *a* and *b* changed dramatically over time in treated tumors, even though treatment resulted in tumor stasis with little to no change in TV during the treatment period. Thus, the *a* and *b* parameters may provide unique insight during monitoring of treatment response, which could supplement measurements of TV. This is important, as anatomic tumor size is currently the only available marker for measuring treatment response

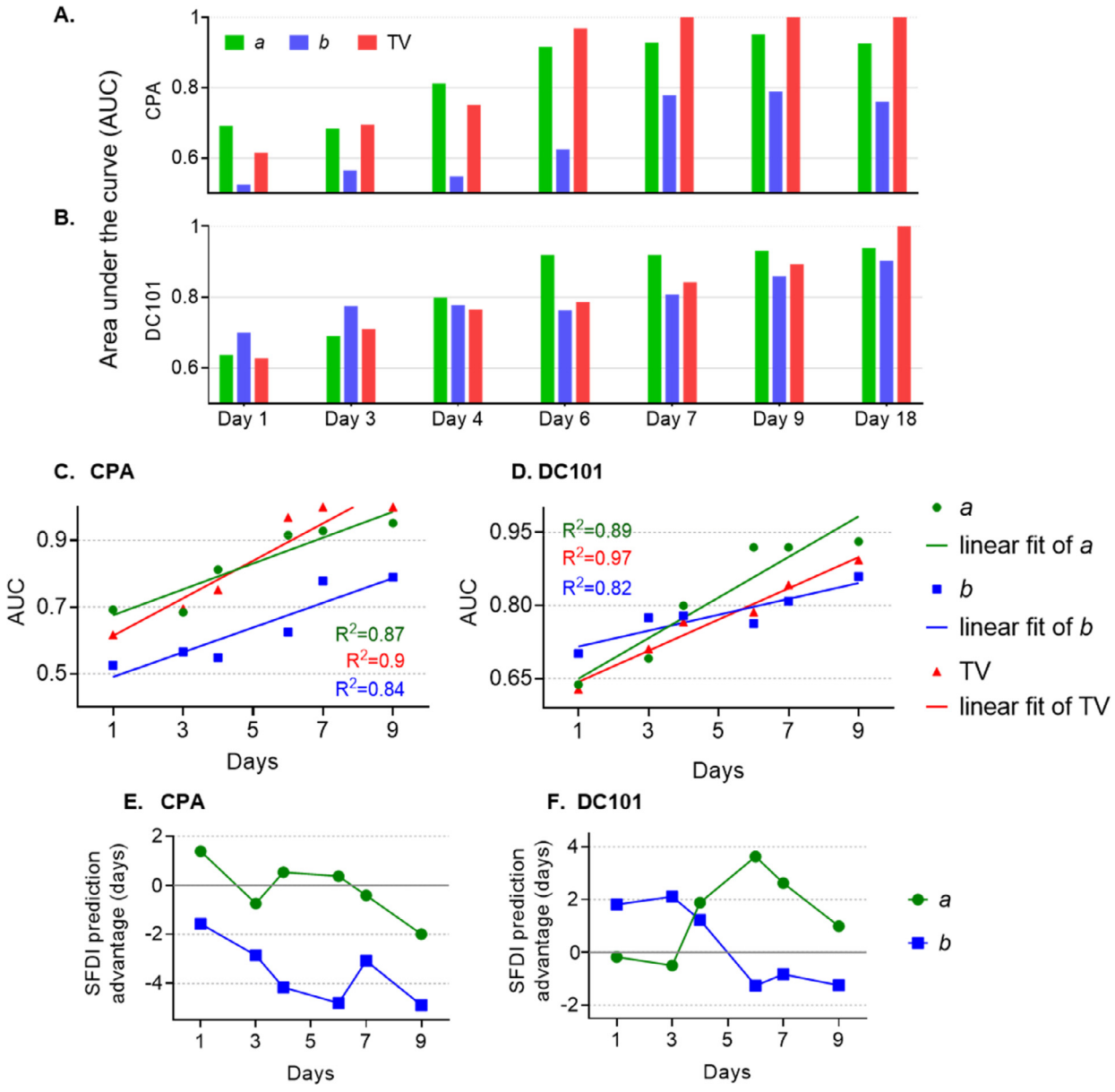

Fig. 5. (A, B) Discriminant classification analysis for discrimination of treated versus control tumors. Area Under the Curve (AUC) values of well-performing stand-alone features are shown in A for CPA and in B for DC101. Corresponding Receiver-Operating Characteristic (ROC) curves are shown in Supplementary Fig. S7. (C, D) AUC values up to day 9 and their linear regression fits for CPA and DC101. (E, F) Regression fits from C and D were used to calculate the predictive advantage (in days) for the *a* or *b* parameter compared to TV. A positive predictive advantage indicates the SFDI feature precedes TV by the indicated number of days. AUC, area under the curve; CPA, cyclophosphamide; SFDI, spatial frequency domain imaging.

in many cancers, and often performs poorly as a marker of treatment response [35].

We also observed a rebound response following cessation of treatment. For example, the *a* parameter increased until the 6-day CPA treatment schedule was discontinued on day 24, and then decreased at day 27 ($P = 0.089$). This decrease correlated with a rebound in TV, which doubled by day 27 (Fig. 3A). In contrast, TVs did not substantially rebound for the DC101-treated tumors after the end of treatment, which likely explains the continued increase in the *a* parameter up to day 27. While these observations suggest that SFDI measurements may be able to detect tumor rebound, the number of tumors remaining at day 27 was small ($n = 2$), and further study with a larger number of tumors would be warranted in the future.

There is little prior work using optical scattering for in vivo tracking of chemotherapy or antiangiogenic treatment response. Most prior studies using DOI modalities have focused on absorption-based parameters, including hemoglobin, water, and lipids, and many clinical Near -Infrared Spectroscopy (NIRS) systems are not capable of quantifying optical scattering [20,22,28,29,32,36–38]. While still less common than NIRS, an increasing number of academic groups have developed clinical frequency-domain systems for tumor measurements, and there is at least 1 commercially available product, although there is not yet an FDA-approved product for this application [39]. We submit that multi-wavelength frequency-domain or time domain clinical modalities are required to measure the *a* and *b* parameters.

While optical scattering provided the strongest predictive advantage during treatment monitoring, absorption-based parameters demonstrated several strong correlations with IHC markers. The blood vessel density marker CD31 correlated strongly with the SFDI-derived hemoglobin parameters ctHbO2 ($\rho_p = 0.85$), ctTHb ($\rho_p = 0.71$), and StO_2 ($\rho_p = 0.92$); and the Hoechst marker for blood vessel patency correlated well with $ctHbO_2$ ($\rho_p = 0.54$), ctTHb ($\rho_p = 0.54$), and StO_2 ($\rho_p = 0.52$). Prior work also reported positive correlations between ctTHb, $ctHbO_2$ and the mean vessel-area marker CD34 [30,31]. We hypothesize that a higher number of functional blood vessels is likely to increase blood distribution in the tumor, which causes the hemoglobin concentration values to increase. The ctHb parameter showed a strong correlation with PCNA ($\rho_p = 0.72$), and we hypothesize that increases in tumor cell proliferation lead to increases in oxygen consumption, resulting in an increase in ctHb [29]. The relatively poor optical contrast observed between treated and untreated tumors in SFDI hemodynamic parameters (Supplementary Fig. S6C, D) may be a reflection of hypoxia within the control group induced by rapid tumor growth, which outpaces vascular supply [40]. This could result in similar decreasing hemodynamic trends in both treated and control groups, but with different biological origins.

While SFDI offers several distinct advantages over other preclinical oncologic imaging modalities, including the fact that it is label-free and provides quantitative optical absorption and scattering contrasts, it also has several notable limitations. SFDI imaging penetration-depth is relatively superficial (<5 mm), and is therefore best suited to superficial tumors. Notably, the optical contrasts measured with SFDI may be translated to the clinic with clinical frequency-domain or time-domain DOI tools. Although less common than simpler continuous-wave NIRS systems, frequency-domain and time-domain DOI systems have undergone significant technical development and clinical testing over the last 2 decades, suggesting they may become viable standard-of-care tools in the near future [39]. SFDI also does not provide tomographic imaging in the implementation used here, although we have used a multi-layer model to remove the effect of overlying skin on imaging [41]. Other study limitations include the statistical correlative nature of our findings, which does not provide a definitive mechanistic link between SFDI-derived parameters and the biological parameters determined by IHC. Additionally, the tumors measured here were relatively large and highly cellular, and the effects of the tumor microenvironment may alter optical signatures differently in human tumors. Finally, both absorption and scattering changes may manifest differently for different therapeutic agents and tumor types. Despite these limitations, our results are supported by prior preclinical and clinical observations, while adding significantly to the current knowledge-base regarding the imaging of treatment response, in particular in animal models.

Going forward, our findings have several potential implications. First, optical scattering has the potential to serve as a new marker of anticancer treatment response in the preclinical setting. The strong correlations between SFDI imaging markers and IHC markers shown here lay the groundwork for the use of SFDI for tracking response to a variety of therapeutic agents with different biological mechanisms. Finally, SFDI could also be used to test new drugs, drug combinations, and therapeutic strategies including adaptive therapies in the preclinical setting.

Conclusion

We have shown here that optical scattering, measured with SFDI, is a new label-free contrast mechanism for tracking treatment response in preclinical tumors models. The scattering parameters a and b were shown to track tumor responses to both cytotoxic and antiangiogenic therapies, respectively, potentially due to their respective sensitivities to apoptosis and proliferation. Optical scattering remains largely unexplored in the context of treatment monitoring in the clinic, and our findings suggest optical scattering should be further investigated with clinical DOI tools. Going forward, widefield measurements of quantitative optical scattering measured with SFDI may represent a powerful new contrast for exploring new drugs and therapeutic strategies in the preclinical setting.

Competing interests

All authors declare that they have no competing financial or nonfinancial interests that might have influenced the performance or presentation of the work described in this manuscript.

Authors' Contributions

Syeda Tabassum: Conceptualization; Data curation; Formal analysis; Investigation; Methodology; Project administration; Software; Validation; Visualization; Roles/Writing – original draft; Writing – review & editing. Anup Tank: Data curation; Formal analysis; Investigation; Methodology; Software.Fay Wang: Data curation; Formal analysis; Software; Visualization; Roles/Writing – review & editing. Kavon Karrobi: Data curation; Investigation; Methodology; Validation; Roles/Writing – review & editing.

Cameron Vergato: Data curation; Formal analysis. Irving J. Bigio: Conceptualization; Methodology; Resources; Supervision; Validation; Visualization; Roles/Writing – review & editing. David Waxman: Conceptualization; Methodology; Resources; Supervision; Validation; Visualization; Roles/ Writing – review & editing. Darren Roblyer: Conceptualization; Data curation; Formal analysis; Funding acquisition; Investigation; Methodology; Project administration; Resources; Software; Supervision; Validation; Visualization; Roles/Writing – original draft; Writing – review & editing.

Funding

The authors gratefully acknowledge funding from the Department of Defense (award no. W81XWH-15-1-0070) and the American Cancer Society (award no. RSG14-014-01-CCE).

Supplementary materials

Supplementary material associated with this article can be found, in the online version, at doi:10.1016/j.neo.2021.01.005.

References

[1] De Jong M, Essers J, Van Weerden WM. Imaging preclinical tumour models: improving translational power. *Nat Rev Cancer* 2014;**14**:481–93.

[2] Conway JRW, Carragher NO, Timpson P. Developments in preclinical cancer imaging: innovating the discovery of therapeutics. *Nat Rev Cancer* 2014;**14**:314–28.

[3] Weissleder R, Pittet MJ. Imaging in the era of molecular oncology. *Nature* 2008;**452**:580–9.

[4] Mulvey CS, Zhang K, Liu W-HB, Waxman DJ, Bigio IJ. Wavelength-dependent backscattering measurements for quantitative monitoring of apoptosis, Part 1: early and late spectral changes are indicative of the presence of apoptosis in cell cultures. *J Biomed Opt* 2011;**16**:117001.

[5] Mourant JR, Freyer JP, Hielscher AH, Eick AA, Shen D, Johnson TM. Mechanisms of light scattering from biological cells relevant to noninvasive optical-tissue diagnostics. *Appl Opt* 1998;**37**:3586–93.

[6] de Bruin DM, Broekgaarden M, van Gemert MJC, Heger M, de la Rosette JJ, Van Leeuwen TG, Faber DJ. Assesment of apoptosis induced changes in scattering using optical coherence tomography. *J Biophotonics* 2016;**9**:913–23.

[7] Farhat G, Giles A, Kolios MC, Czarnota GJ. Optical coherence tomography spectral analysis for detecting apoptosis in vitro and in vivo. *J Biomed Opt* 2015;**20**:126001.

[8] Chung SH, Feldman MD, Martinez D, Kim H, Putt ME, Busch DR, Tchou J, Czerniecki BJ, Schnall MD, Rosen MA, DeMichele A, Yodh AG, Choe R. Macroscopic optical physiological parameters correlate with microscopic proliferation and vessel area breast cancer signatures. *Breast Cancer Res* 2015;**17**(1).

[9] Hu W, Kavanagh JJ. Anticancer therapy targeting the apoptotic pathway. *Lancet Oncol* 2003;**4**:721–9.

[10] Lowe SW, Lin AW. Apoptosis in cancer. *Carcinogenesis* 2000;**21**:485–95.

[11] Waxman DJ, Schwartz PS. Harnessing apoptosis for improved anticancer gene therapy. *Cancer Res* 2003;**63**:8563–72.

[12] Reed JC. Apoptosis-targeted therapies for cancer. *Cancer Cell* 2003;**3**(1):17–22.

[13] Wyllie AH, Kerr JF, Currie AR. Cell death: the significance of apoptosis. *Int Rev Cytol* 1980;**68**:251–306.

[14] Kerr JFR, Wyllie AH, Currie AR. Apoptosis: a basic biological phenomenon with wide-ranging implications in tissue kinetics. *Br J Cancer* 1972;**26**:239–57.

[15] Vander Heiden MG, Chandel NS, Williamson EK, Schumacker PT, Thompson CB. Bcl-x(L) regulates the membrane potential and volume homeostasis of mitochondria. *Cell* 1997;**91**:627–37.

[16] Desagher S, Martinou JC. Mitochondria as the central control point of apoptosis. *Trends Cell Biol* 2000;**10**(9):369–77.

[17] Mulvey CS, Liu W-H, Bigio IJ, Zhang K, Waxman DJ. Wavelength-dependent backscattering measurements for quantitative monitoring of apoptosis, Part 2: early spectral changes during apoptosis are linked to apoptotic volume decrease. *J Biomed Opt* 2011;**16**:117002.

[18] Cuccia DJ, Bevilacqua F, Durkin AJ, Ayers FR, Tromberg BJ. Quantitation and mapping of tissue optical properties using modulated imaging. *J Biomed Opt* 2009;**14**:024012.

[19] Muldoon TJ, Roblyer D, Williams MD, Stepanek VM, Richards-Kortum R, Gillenwater AM. Noninvasive imaging of oral neoplasia with a high-resolution fiber-optic microendoscope. *Head Neck* 2012;**34**:305–12.

[20] Ueda S, Roblyer D, Cerussi A, Durkin A, Leproux A, Santoro Y, Xu S, O'Sullivan TD, Hsiang D, Mehta R, Butler J, Tromberg BJ. Baseline tumor oxygen saturation correlates with a pathologic complete response in breast cancer patients undergoing neoadjuvant chemotherapy. *Cancer Res* 2012;**72**:4318–28.

[21] Tromberg BJ, Zhang Z, Leproux A, O'Sullivan TD, Cerussi AE, Carpenter PM, Mehta RS, Roblyer D, Yang W, Paulsen KD, Pogue BW, Jiang S, Kaufman PA, Yodh AG, Chung SH, Schnall M, Snyder BS, Hylton N, Boas DA, Carp SA, Isakoff SJ, Mankoff D. Predicting responses to neoadjuvant chemotherapy in breast cancer: ACRIN 6691 trial of diffuse optical spectroscopic imaging. *Cancer Res* 2016;**76**:5933–44.

[22] Schaafsma BE, van de Giessen M, Charehbili A, Smit VTHBM, Kroep JR, Lelieveldt BPF, Liefers G-J, Chan A, Lowik CWGM, Dijkstra J, van de Velde CJH, Wasser MNJM, Vahrmeijer AL. Optical mammography using diffuse optical spectroscopy for monitoring tumor response to neoadjuvant chemotherapy in women with locally advanced breast cancer. *Clin Cancer Res* 2015;**21**:577–84.

[23] He J, Li CL, Wilson BC, Fisher CJ, Ghai S, Weersink RA. A clinical prototype transrectal diffuse optical tomography (TRDOT) system for in vivo monitoring of photothermal therapy (PTT) of focal prostate cancer. *IEEE Trans Biomed Eng* 2020;**67**(7):2119–29.

[24] Tabassum S, Zhao Y, Istfan R, Wu J, Waxman DJ, Roblyer D. Feasibility of spatial frequency domain imaging (SFDI) for optically characterizing a preclinical oncology model. *Biomed Opt Express* 2016;**7**:4154–70.

[25] Zhang K, Waxman DJ. Impact of tumor vascularity on responsiveness to antiangiogenesis in a prostate cancer stem cell-derived tumor model. *Mol Cancer Ther* 2013;**12**:787–98.

[26] Mourant JR, Fuselier T, Boyer J, Johnson TM, Bigio IJ. Predictions and measurements of scattering and absorption over broad wavelength ranges in tissue phantoms. *Appl Opt* 1997;**36**:949.

[27] Beauvoit B, Liu H, Kang K, Kaplan PD, Miwa M, Chance B. Characterization of absorption and scattering properties for various yeast strains by time-resolved spectroscopy. *Cell Biophys* 1993;**23**:91–109.

[28] Soliman H, Gunasekara A, Rycroft M, Zubovits J, Dent R, Spayne J, Yaffe MJ, Czarnota GJ. Functional imaging using diffuse optical spectroscopy of neoadjuvant chemotherapy response in women with locally advanced breast cancer. *Clin Cancer Res* 2010;**16**:2605–14.

[29] Cerussi A, Hsiang D, Shah N, Mehta R, Durkin A, Butler J, Tromberg BJ. Predicting response to breast cancer neoadjuvant chemotherapy using diffuse optical spectroscopy. *Proc Natl Acad Sci U S A.* 2007;**104**:4014–19.

[30] Srinivasan S, Pogue BW, Brooksby B, Jiang S, Dehghani H, Kogel C, Wells WA, Poplack SP, Paulsen KD. Near-infrared characterization of breast tumors in vivo using spectrally-constrained reconstruction. *Technol Cancer Res Treat* 2005;**4**:513–26.

[31] Zhu Q, Kurtzman SH, Hegde P, Tannenbaum S, Kane M, Huang M, Chen NG, Jagjivan B, Zarfos K. Utilizing optical tomography with ultrasound localization to image heterogeneous hemoglobin distribution in large breast cancers. *Neoplasia* 2005;**7**:263–70.

[32] Roblyer D, Ueda S, Cerussi A, Tanamai W, Durkin A, Mehta R, Hsiang D, Butler JA, McLaren C, Chen W-P, Tromberg B. Optical imaging of breast cancer oxyhemoglobin flare correlates with neoadjuvant chemotherapy response one day after starting treatment. *Proc Natl Acad Sci U S A* 2011;**108**:14626–31.

[33] Cocco RE, Ucker DS. Distinct modes of macrophage recognition for apoptotic and necrotic cells are not specified exclusively by phosphatidylserine exposure. *Mol Biol Cell* 2001;**12**:919–30.

[34] Nguyen QD, Lavdas I, Gubbins J, Smith G, Fortt R, Carroll LS, Graham MA, Aboagye EO. Temporal and spatial evolution of therapy-induced tumor apoptosis detected by caspase-3-selective molecular imaging. *Clin Cancer Res* 2013;**19**:3914–24.

[35] Yeh E, Slanetz P, Kopans DB, Rafferty E, Georgian-Smith D, Moy L, Halpern E, Moore R, Kuter I, Taghian A. Prospective comparison of mammography, sonography, and MRI in patients undergoing neoadjuvant chemotherapy for palpable breast cancer. *Am J Roentgenol* 2005;**184**:868–77.

[36] Jiang S, Pogue BW, Kaufman PA, Gui J, Jermyn M, Frazee TE, Poplack SP, DiFlorio-Alexander R, Wells WA, Paulsen KD. Predicting breast tumor response to neoadjuvant chemotherapy with diffuse optical spectroscopic tomography prior to treatment. *Clin Cancer Res* 2014;**20**:6006–15.

[37] Pogue BW, Poplack SP, McBride TO, Wells WA, Osterman KS, Osterberg UL, Paulsen KD. Quantitative hemoglobin tomography with diffuse near-infrared spectroscopy: pilot results in the breast. *Radiology* 2001;**218**:261–6.

[38] Zhu Q, Tannenbaum S, Hegde P, Kane M, Xu C, Kurtzman SH. Noninvasive monitoring of breast cancer during neoadjuvant chemotherapy using optical tomography with ultrasound localization. *Neoplasia* 2008;**10**:1028–40.

[39] Durduran T, Choe R, Baker WB, Yodh AG. Diffuse optics for tissue monitoring and tomography. *Reports Prog Phys* 2010;**73**:076701.

[40] Jain RK. Normalization of tumor vasculature: an emerging concept in antiangiogenic therapy. *Science* 2005;**307**(5706):58–62.

[41] Tabassum S, Pera V, Greening G, Muldoon TJ, Roblyer D. Two-layer inverse model for improved longitudinal preclinical tumor imaging in the spatial frequency domain. *J Biomed Opt* 2018;**23**:1–12.